Tellus (2004), 56B, 249–261
Printed in UK. All rights reserved

TELLUS

Retrieving N_2O from nadir-viewing infrared spectrometers

By A. M. LUBRANO[1], G. MASIELLO[2], M. MATRICARDI[3], C. SERIO[1]* and V. CUOMO[2],
[1]*Istituto Nazionale per la Fisica della Materia, Unità di Napoli, Gruppo Coordinato di Potenza, C.da Macchia Romana, 85100 Potenza, Italy;* [2]*Istituto di Metodologie Avanzate di Analisi Ambientale del CNR, Tito Scalo, Pz, Italy;* [3]*European Centre for Medium-Range Weather Forecasts, ECMWF, Shinfield Park, Reading, Berkshire RG2 9AX, UK*

(Manuscript received 14 February 2003; in final form 30 October 2003)

ABSTRACT

The paper describes and demonstrates a methodology for the physical retrieval of nitrous oxide that uses the spectral radiance measured by the next generation of high-resolution satellite-borne infrared sensors. The performance of the retrieval scheme has been assessed on the basis of numerical exercises. Examples of retrievals based on Interferometric Monitoring of Greenhouse Gases (IMG) spectra measured over the sea surface are given to demonstrate the ability of the scheme to obtain accurate N_2O concentration values.

1. Introduction

Nitrous oxide (N_2O) is an important greenhouse gas with an atmospheric lifetime of 120 yr. It is mostly produced by microbial processes in soil and increases with intensified land use, especially as a result of fertilization. Nitrous oxide plays an important role in atmospheric chemistry: in addition to being radiatively active in the infrared, and therefore an important greenhouse gas, the dissociation of N_2O by excited oxygen atoms is the major source of nitrogen oxides (NO_x = NO, NO_2), which are important in determining the distribution of both tropospheric and stratospheric ozone (Liou, 1992).

The N_2O level in the lower troposphere is monitored by the Climate Monitoring and Diagnostic Laboratory (CMDL) of the National Oceanic and Atmospheric Administration (NOAA) through measurements made at a world-wide distributed network of stations (for further information see http://www.cmdl.noaa.gov). The most updated and accurate survey on chemically and radiatively important gases in the atmosphere has been provided in the context of the Advanced Global Atmospheric Gas Experiment (AGAGE). AGAGE (Prinn et al., 2000) sets the present value of N_2O mixing ratio at ≈0.32 parts per million by volume (ppmv) and indicates that the global average trend in N_2O lies in the range from 0.25 to 0.31% yr^{-1}. The analysis also evidenced a latitudinal gradient and a small but statistically significant annual cycle in N_2O.

Despite the very low long-term trend in N_2O concentration, as a likely result of intensified land use and anthropogenic activities, *in situ* measurements show a short-term variability (day-to-day, month-to-month) in N_2O, which can reach peak-to-peak oscillations of magnitude of ±5–7% around the annual mean. This combination of natural and anthropogenic variability is seen both in unpolluted sites and close to anthropogenic sources. It is, for example, quite clear in the hourly and monthly records from Cape Matatulu station (which is also a station of the AGAGE net) and the Lampedusa station to the south of the Mediterranean Sea (WMO, 2001). Also interesting is the fact that high-altitude stations, e.g. Plateau Rosa (≈3500 m), show a relatively high variability for N_2O concentration even in the monthly means (see http://www.cesi.it/greeninfo/monitoraggio), which exemplifies how this variability is not limited to the boundary layer but involves the free troposphere as well. It is not clear at the moment whether or not this short-timescale variability is paralleled by an equivalent spatial variability, which makes global coverage observations highly desirable.

Given the current and future availability of satellite observations at high spatial resolution, we have examined in this paper the feasibility of N_2O retrieval from space. A strategy for the physical retrieval of N_2O profiles is described which applies to the current and future generation of high-resolution infrared sounders as the Atmospheric Infrared Sounder (AIRS) on the AQUA satellite (launched in 2002), the Geosynchronous Imaging Fourier Spectrometer (GIFTS) on the EO-3 platform (to be launched in 2005), the Infrared Atmospheric Sounding Interferometer (IASI) on the METOP platform (to be launched in 2005) and the Cross Track Infrared Sounder (CrIS) on the NPP (launch

*Corresponding author.
e-mail: serio@unibas.it

date 2006) and NPOESS (to be launched in 2008) satellites. All these spectrometers are characterized by a broad-band spectral coverage (≈3.7 to 15.5 μm) and a spectral sampling rate in the range 0.25 to 1 cm^{-1}.

Two inversion schemes have been developed and tested. The first one is based on a non-parametric estimation approach where no special assumptions other than the ones contained in the first guess are made about the shape of the N_2O profile. In the second scheme, however, the observed profile is parametrized in terms of the reference vertical concentration and therefore results in a smaller number of degrees of freedom in the final solution. Since N_2O is a well-mixed gas, it will be shown that the parametric estimation approach performs as well as the non-parametric one.

The retrieval of the concentration of an atmospheric gas from infrared radiance requires an *a priori* knowledge of the temperature profile. Because of the wide spectral range covered by the new generation of infrared sensors, the temperature profile can be obtained from the inversion of the spectral radiance in suitable spectral ranges and then used to perform the retrieval of the concentration of the gas species by using the radiance measured in a different (and not-overlapping) spectral region. In this paper we have used the following approach. The CO_2 absorption band at 14 μm is used with part of the atmospheric window at 11 μm (the 800 to 830 cm^{-1} and 1100 to 1200 cm^{-1} spectral regions rich in weak water vapour lines) to perform the simultaneous retrieval of the temperature and water vapour profiles. This information is then used in a sequential retrieval approach to retrieve the N_2O profile using a portion of its ν_3 fundamental band at 4.5 μm.

To demonstrate the ability of the method to retrieve N_2O concentration profiles from space, a set of IMG spectra have been used. The Interferometric Monitoring of Greenhouse Gases (IMG) instrument (Kobayashi et al. 1999) flew on board the Japanese Advanced Earth Observing Satellite (ADEOS) from October 1996 to June 1997. The instrument is a Fourier transform spectrometer that observes Earth's emission spectrum at nadir in three spectral bands from 3.3 to 16 μm with a nominal spectral sampling of 0.05 cm^{-1}.

The paper is organized as follows. Section 2 describes the choice of the spectral range used for the retrieval of N_2O, the strategy for the inversion and summarizes the details relevant to the radiative transfer calculations. Section 3 describes the physical retrieval approach and gives an assessment of its performance. Section 4 shows examples of retrievals based on IMG spectra. Conclusion are drawn in Section 5.

2. The inversion strategy and background

To perform the retrieval of N_2O profiles we need

(1) a radiative transfer model to simulate the observed radiance spectrum,

(2) a suitable spectral range that is mostly sensitive to N_2O and where contamination from other absorbing gases is negligible,

(3) information about temperature and water vapour vertical distribution.

These three basic aspects will be discussed here.

2.1. *Radiative transfer calculations*

All the radiative transfer calculations presented in this paper have been performed using the σ-IASI code (Amato et al., 2002), a fast line-by-line model that, in addition to spectral radiance, can compute analytical Jacobians for the major geophysical parameters (e.g. temperature, water vapour, ozone, carbon dioxide, nitrous oxide). Although the code has been developed mostly for IASI, it is well suited for nadir-viewing satellite and airplane infrared sensors with a sampling rate in the range 0.1–2 cm^{-1}. The code computes monochromatic radiances from look-up tables of monochromatic layer optical depth generated using the line-by-line model LBLRTM (Clough et al., 1992). Following the LBLRTM strategy, for each individual species, the optical depth of the monochromatic layer is generated and stored in the appropriate look-up table at a sampling rate, $\Delta\sigma$, equal to 0.25 times the width of the narrowest gas absorption line, which gives for the highest-altitude layer $\Delta\sigma = 0.000\,169$ cm^{-1}. The code σ-IASI borrows from LBLRTM the CO_2 line mixing scheme. Cross sections of heavy molecules such as chlorofluorocarbons are not parametrized in terms of look-up tables, since absorption can be quickly computed separately. The code σ-IASI accounts for the presence of CFC species, namely CCl3F (CFC-11) and CCl2F2 (CFC-12). Water vapour continuum absorption is computed separately; we use the CKD standard (Clough et al., 1989), version 2.4. The atmospheric layering embedded in σ-IASI consists of a pressure layer grid of $N_l = 44$ grid points (Amato et al., 2002). All the required spectroscopic parameters have been extracted from the HITRAN 96 database (Rothman et al., 1998). Further details about σ-IASI may be found in Amato et al. (2002).

To simulate the observations, the σ-IASI monochromatic radiance is convolved with a pure cardinal sine function, whose parameters are set up to correspond to the instrumental line shape of an ideal interferometer spectrometer of maximum optical delay of 2 cm, and, finally, apodized with a Gaussian function of 0.25 cm^{-1} half-width half-height. For consistency IMG spectra have been apodized with the same function as that used for the synthetic spectral radiance. The sampling rate of the final spectra (simulated and observed) is $\Delta\sigma = 0.25$ cm^{-1}. This choice matches the sampling rate of most of the modern nadir-viewing sensors which are planned to fly in this decade.

The reason for the Gaussian apodization is twofold. First Gaussian apodization is consistent with what for now has been prescribed for the IASI level 1C data, so that our calculations yield IASI-like spectra.

Second, this study is mostly based on IMG spectra whose nominal sampling rate is 0.05 cm^{-1}. However, one has to bear in mind that the spectral response function of IMG is not well characterized: it differs from the theoretical cardinal sine function mostly because of self-apodization. Gaussian apodization (Lubrano et al., 2000) limits the problems of self-apodization and allows us to compare observations and calculations on the basis of a common instrumental line shape. The rationale of the method is that under apodization with a known mathematical function, $w(\sigma)$, the unknown spectral response function, $\tilde{I}(\sigma)$, transforms to

$$I(\sigma) = \int_{-\infty}^{+\infty} \tilde{I}(\sigma_0) w(\sigma - \sigma_0) \mathrm{d}\sigma_0 \quad (1)$$

and we have $I(\sigma) \approx w(\sigma)$ provided that w is much wider than the unknown $\tilde{I}(\sigma)$. To this end, we have used a re-sampling rate $\Delta\sigma = 0.25$ cm^{-1}, which is five times larger than the IMG nominal sampling rate.

To model the observational noise, the covariance matrix of observations undergoes the same kind of transformation (Amato et al., 1998) and therefore is properly scaled to the new sampling rate resolution. In this analysis the covariance matrix has been built up by the IMG radiometric noise figures obtained at the proto flight level. For the spectral range of interest in this study (2195–2215 cm^{-1}) the IMG radiometric noise (noise equivalent difference temperature (NEDT) at the level of unapodized spectral radiance) is ≈1.3 K at a scene temperature of 280 K. After apodization and re-sampling this figure becomes ≈0.33 K at 280 K.

In this study all the radiance spectra have been computed for a nadir view and assuming a sea surface. To compute the emissivity of a sea surface, the Masuda model has been used (Masuda et al., 1988).

2.2. *Choice of the N_2O spectral range*

Nitrous oxide has three main vibrational bands in the infrared centred at 1284.91 cm^{-1} (ν_1), 588.77 cm^{-1} (ν_2) and 2223.76 cm^{-1} (ν_3) respectively. The ν_2 fundamental band is outside the range of current and planned infrared sensors and is therefore not considered here. The ν_1 band overlaps the methane ν_4 band centred at 1310.76 cm^{-1} and the H_2O main vibrational band centred at 1594.75 cm^{-1}. Given the sampling rate (between 0.25 and 2 cm^{-1}) of the sensors considered here, use of the N_2O ν_1 band has to be dismissed since the contribution of H_2O and CH_4 to the observed spectral radiance makes it too difficult to disentangle the concentration of N_2O from that of the other two conflicting gases.

The ν_3 band overlaps in part the ν_3 band of CO_2. However, CO_2 is much less variable than H_2O, methane and N_2O itself. Unless we consider polluted areas, natural infra-annual variability of CO_2 is less than 2% to be compared with an observed peak value of 5–7% (WMO, 2001) for N_2O.

Figure 1a shows the plot of the difference

$$\Delta_1 = S_{\mathrm{ref}}(\sigma) - S_{+}(\sigma) \quad (2)$$

where $S_{\mathrm{ref}}(\sigma)$ is the spectral radiance at a wave number σ computed for a reference tropical air mass (Anderson et al., 1986) and

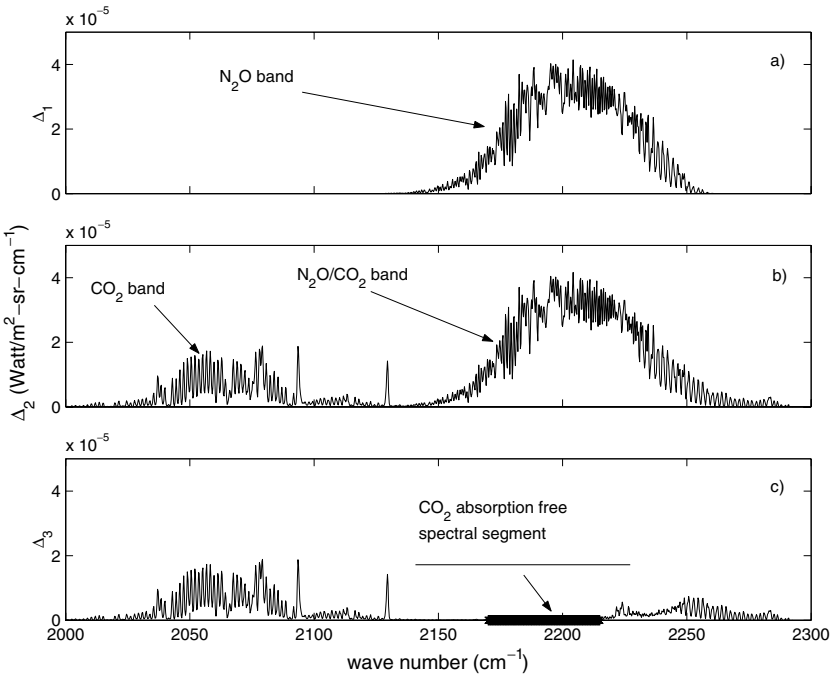

Fig 1. The difference between reference and test spectra for a tropical air mass: (a) the test spectrum is obtained perturbing the N_2O profile by +5%; (b) the test spectrum is obtained perturbing simultaneously the N_2O and CO_2 profiles by +5% and +2% respectively; (c) shows the difference $\Delta_3 = \Delta_2 - \Delta_1$ and evidences how the range 2170 to 2215 cm^{-1} is free from CO_2 absorption.

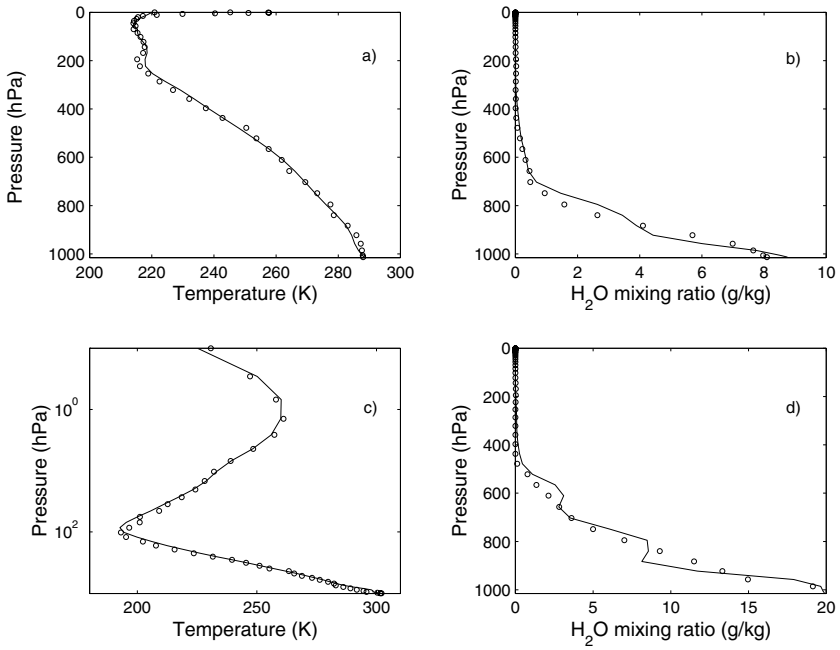

Fig 2. Example of temperature and water vapour profiles retrieved using the scheme discussed in Lubrano et al. (2000). The inversion has been performed using the spectral ranges 667 to 830 cm^{-1} and 1100 to 1200 cm^{-1}. Panels (a) and (b) show the retrieved profiles (circle symbols) for the IMG mid-latitude winter spectrum 327906, Obs.1. Panels (c) and (d) show the retrieval analysis for the IMG tropical spectrum 374126. The temperature profiles in panel (c) is plotted using a logarithmic scale to ease the comparison in the upper atmosphere. For all cases the ECMWF analysis for the same location and date is given as a solid curve.

$S_+(\sigma)$ is the computed spectral radiance for the same atmospheric profile with the N_2O concentration increased by +5% at each layer. The plot of the difference clearly shows the N_2O absorption band which extends from approximately 2150 to 2270 cm^{-1}.

Figure 1b shows the difference (Δ_2 in Fig. 1b) between $S_{\rm ref}(\sigma)$ and $S_+(\sigma)$ where $S_+(\sigma)$ has now been obtained by simultaneously increasing the CO_2 and N_2O profiles by 2% and 5% respectively. The difference $\Delta_3 = \Delta_2 - \Delta_1$ is shown in Fig. 1c. It can be seen that the region 2170–2215 cm^{-1} is not affected by CO_2 absorption (at least at the sampling rate of 0.25 cm^{-1}). The region 2170–2195 cm^{-1} still has some important water vapour spectral features. In order to minimize the possible interference from water vapour, we selected the spectral region used for the retrieval of N_2O to be in the range 2195–2215 cm^{-1}.

2.3. *Temperature and water vapour information*

Atmospheric gas retrieval in the infrared depends critically on the vertical distribution of temperature. In addition, absorption from water vapour can also be important because of its potential interfering effects. The strategy we have devised is to adopt a sequential retrieval scheme in which skin temperature, temperature and water vapour are simultaneously retrieved at the first step. The spectral ranges used for the retrieval are 645 to 830 cm^{-1} and 1100 to 1200 cm^{-1}. The first spectral interval overlaps the long-wave absorption band of CO_2 and is used here mostly for temperature. The range 1100 to 1200 cm^{-1} provides information about water vapour in the lower and middle atmosphere.

The inversion algorithm used for temperature and water vapour is discussed by Lubrano et al. (2000). As an example, the algorithm has been used to derive the temperature and water vapour profiles shown in Fig. 2 from a mid-latitude winter IMG spectrum (panels a and b) and from a tropical IMG spectrum (panels c and d), respectively. Also shown in the figure is the temperature and H_2O profile provided by the analysis from the European Centre for Medium Range Weather Forecasts (ECMWF). Note that above 10 hPa the ECMWF temperature profile is supplemented with the temperature profile retrieved by the national Environmental Satellite Data and Information Service (NESDIS). This is because at the time the IMG spectra were recorded, the top of the vertical pressure grid used in the ECMWF global atmospheric model was placed at 10 hPa. In Fig. 2c the temperature profile is plotted using a logarithmic scale to ease the comparison in the upper atmosphere. The mid-latitude winter type IMG spectrum was recorded over the Mediterranean Sea on 3 April 1997, at UTC 21:36:00.88, whereas the tropical spectrum was recorded over the Indian Ocean on 6 May 1977, UTC: 07:18:24.93. The two IMG spectra were resampled at the sampling rate of 0.25 cm^{-1} before inversion for temperature and water vapour. Both spectra will be used again in Section 4 to exemplify the application of the N_2O retrieval methodology to real observations.

3. N_2O retrieval methodology and analyses

3.1. *Non-parametric approach*

Nitrous oxide is retrieved at the $N_l = 44$ pressure-grid points of σ-IASI, according to the regularized inverse equation, e.g. (Carfora et al., 1998)

$$\delta\hat{\mathbf{q}} = (\mathbf{K}'\mathbf{S}^{-1}\mathbf{K} + \gamma\mathbf{B}^{-1})^{-1}\mathbf{K}'\mathbf{S}^{-1}\delta\mathbf{r} \tag{3}$$

with the prime indicating *transpose* and where

(1) $\delta\mathbf{r} = \mathbf{r} - \mathbf{r}_0$; with $\mathbf{r}$ the observed radiance vector and $\mathbf{r}_0$ *the reference* or first guess radiance vector.

(2) $\delta\hat{\mathbf{q}} = \hat{\mathbf{q}} - \mathbf{q}_0$; with $\mathbf{q}$ the estimated N_2O concentration vector and $\mathbf{q}_0$ the *reference* or first guess N_2O concentration vector.

(3) $\mathbf{S}$ is the covariance matrix of the observations.

(4) $\mathbf{K}$ is the N_2O Jacobian or derivative matrix computed at $\mathbf{q}_0$.

(5) $\mathbf{B}$ is a smoothing operator.

(6) γ is the regularization parameter.

The smoothing operator $\mathbf{B}$ is here defined to be the exponential covariance function:

$$B(i, j) = v_i v_j \exp\left(-\frac{|\, p_i - p_j \,|}{\Delta p}\right) \tag{4}$$

with p_i the pressure value at the ith point of the pressure layer grid. In this study we have chosen $\Delta p = 1.3$ hPa which gives a quasi-diagonal $\mathbf{B}$ matrix whose diagonal elements are $(v_1, \ldots, v_{N_1}) = \mathbf{v} = 0.2\ \mathbf{q}_0$ which means that the expected variability of the N_2O profile is within 20% of its reference value $\mathbf{q}_0$. This choice is empirical and is not based on real observations that for N_2O are rare (at least as far as its vertical distribution is concerned). The nature of this constraint is rather mathematical than statistical. For this reason we also include an additional smoothing parameter, γ, in order to optimally tune the smoothness of the final solution. The optimal value of γ is chosen by using the so-called L-curve criterion (Hansen, 1992).

Finally, the covariance matrix of the observations $\mathbf{S}$ is defined based on the radiometric noise figure for IMG. Once the covariance matrix $\mathbf{S}$ is specified, the covariance matrix $\mathbf{C}$ used in the inversion process is derived from eq. (3), e.g. (Kendall and Stuart, 1979)

$$\mathbf{C} = \left(\mathbf{J}'\mathbf{J} + \gamma_{\text{opt}}\mathbf{B}^{-1}\right)^{-1}\mathbf{J}'\mathbf{J}\left(\mathbf{J}'\mathbf{J} + \gamma_{\text{opt}}\mathbf{B}^{-1}\right)^{-1} \tag{5}$$

where $\mathbf{J}$ is the normalized Jacobian, $\mathbf{J} = \mathbf{S}^{-\frac{1}{2}}\mathbf{K}$, and γ_{opt} is the optimal value of the regularization parameter.

Assessment of the profiling accuracy The analysis presented here uses the TIGR database (Chedin et al., 1985) in the form made available to the IASI Sounding Science Working Group (ISSWG). This database consists of a set of 2311 radiosonde profiles for temperature and water vapour supplemented by a set of 383 ozone profiles from the NESDIS.

For the assessment of the performance of the retrieval scheme, a subset of 100 profiles were selected at random for each type of air mass. We use the usual climatological classification (Anderson et al., 1986) for the air mass: tropical, mid-latitude summer, mid-latitude winter, high-latitude summer and high-latitude winter. The total number of selected profiles was therefore 500. Profiles for the minor and trace gases were obtained from the Air Force Geophysical Laboratory (AFGL) compilation (Anderson et al., 1986).

For each of the 500 selected profiles, synthetic IASI-like radiances were computed using the σ-IASI code. Three basic sets of radiances were generated: the first was obtained by using a reference climatological profile for N_2O whereas the other two were obtained by perturbing the reference N_2O profile by $\pm 5\%$.

The N_2O mixing ratio profile after perturbation $q(p)$ (p here is the pressure) can be written as a function of the reference profile $q_0(p)$ using the following equation:

$$q(p) = q_0(p)(1 + \pi(p)) \tag{6}$$

where the scaling factor $\pi(p)$ can be written as a function of a magnitude f_0 and a scale height h_p

$$\pi(p) = f_0 \exp\left(\frac{p - p_0}{h_p}\right) \tag{7}$$

here p_0 denotes the pressure at ground level. Equation (7) can be used to define the perturbed N_2O profile in the most general way. A systematic perturbation can for instance be obtained by setting $h_p = \infty$. By properly assigning the scale height we can simulate perturbations that occur at low altitudes or in localized regions such as those expected to be generated in the lower atmosphere because of anthropogenic activities. However, later in this and the next section we will show that we are only able to retrieve a perturbed profile that has been assigned a scale height that tends to infinity: perturbations localized at low altitudes cannot be resolved in the infrared unless we use spectra measured over surfaces with a very low emissivity.

It should be stressed here that given the long lifetime of N_2O we expect the gas to be well mixed so that we can reasonably assume that the shape of the profile is known: we are looking for the occurrence of a shift with respect to a reference value.

Keeping this in mind, the perturbed data set was used to generate the observations (addition of observational noise consistent to the covariance matrix specified in the previous section). Using the reference set as the first guess, the perturbed N_2O profiles were retrieved according to the sequential methodology outlined above, that is:

- The radiance in the spectral intervals 645–830 cm^{-1} and 1100–1200 cm^{-1} is used to retrieve the temperature and water vapour profiles.
- The N_2O profile is retrieved using the radiance in the spectral interval 2195 to 2215 cm^{-1} and the temperature and water vapour profile retrieved at the first step.

For each given air mass type, the retrieved profiles were then compared with the test profiles to compute the root mean square (rms) error defined as:

$$e(p_i) = \left(\frac{1}{N_{\text{obs}}}\sum_{j=1}^{N_{\text{obs}}}\left(\hat{q}^{(j)}(p_i) - q^{(j)}(p_i)\right)^2\right)^{\frac{1}{2}} \tag{8}$$

where $N_{\text{obs}} = 100$, $\hat{q}^{(j)}(p_i)$ is the retrieved concentration for the sample j at the ith level pressure p_i, and $q^{(j)}(p_i)$ is the corresponding test value.

Figure 3 shows, for the various air mass types and for an N_2O perturbation of +5%, the vertical distribution of the rms

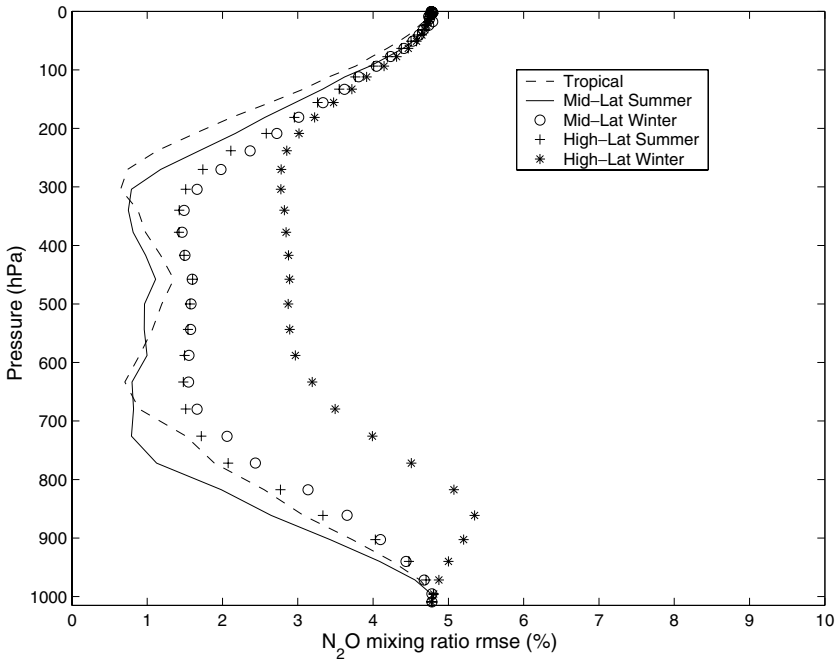

Fig 3. The accuracy of the retrieval scheme for a test case where the N_2O concentration profile is equal to 1.05 times its climatological value (+5% perturbation). The figure shows the N_2O retrieval accuracy in terms of the root mean square error (rmse) for the various air mass types.

error. It can be seen that in the lower and upper atmosphere the error almost coincides with the magnitude of the perturbation, which means that there is no sensitivity to N_2O variations in the boundary layer or in the upper atmosphere. However, for pressures between 300 and 700 hPa the accuracy is of the order of 1% for the mid-latitude summer and tropical air masses, 1.5–2% for the mid-latitude winter and high-latitude summer air masses and around 3–4% for high-latitude winter air masses. We can thus conclude that with the exception of the high-latitude winter air masses the N_2O concentration profile between 300 and 700 hPa can be retrieved with a reasonable level of accuracy. The error analysis for the -5% perturbation case gives similar results. In general, results show that for a perturbation of $\pm 5\%$ the N_2O profile can be retrieved with a rms accuracy better than 2% for pressures between 300 and 700 hPa.

The sensitivity of the radiance to profile perturbation is shown in Fig. 4a, where the Jacobian for a tropical air mass is plotted. It can be seen that the Jacobian peaks at pressures between 300 and 700 hPa and then attains very low values for pressures either side of this range. Thus the low sensitivity to a perturbation in the boundary layer is intrinsic to the physical processes that govern the radiative transfer in the spectral range considered. However, it should be said that our analysis applies to the sea surface where the spectral emissivity is ≈ 1 or very close to 1 in the infrared. For surfaces characterized by a lower spectral emissivity, the performance of the retrieval scheme in the boundary layer is expected to improve.

To see how emissivity can influence the sensitivity of the retrieval in the boundary layer, let us consider the derivative of the spectral radiance with respect to the gas concentration q_1 in the lowest atmospheric layer. If $R(\sigma)$ is the monochromatic spectral

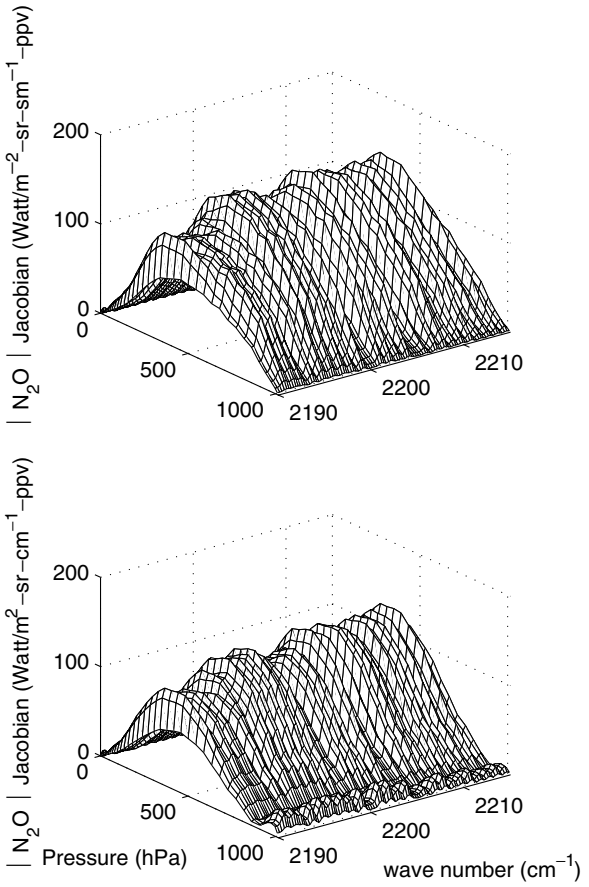

Fig 4. Absolute value of the N_2O Jacobian for a typical tropical air mass. The upper panel is for sea surface emissivity, whereas the lower panel refers to a bare soil (desert) emissivity.

radiance, then by retaining only the leading terms of the derivative of the radiance with respect to q_1 (e.g. Amato et al., 2002) we can write

$$\frac{\partial R(\sigma)}{\partial q_1} = [-\varepsilon_0 \tau_0 P(T_g) + \tau_0 P(T_l)] \frac{\partial \nu_1}{\partial q_1} \quad (9)$$

where ν_1 is the monochromatic layer optical depth for the considered gas species, P is the Planck function, T_g and T_l are the surface and the average layer temperature, respectively; τ_0 is the total transmittance from the surface to the top of the atmosphere and finally ε_g is the spectral emissivity of the surface. For a sea surface we have typically $T_g \approx T_l$, so that if $\varepsilon_0 \approx 1$, we have ε_0 τ_0 $P(T_g) \approx \tau_0$ $P(T_1)$ and the derivative is very close to zero: a change of concentration of N_2O at low altitudes is hard to detect from space in the infrared.

Equation (9) applies to monochromatic radiance, therefore the sensitivity of the retrieval in the lower layers cannot be improved by increasing the spectral resolution of the sensor. This can only be achieved by making ε_0 significantly lower than 1, i.e. the sensor has to look at low-emissivity surfaces. In addition, it should be stressed that since eq. (9) applies to any atmospheric gas, the accuracy of the retrieval in the presence of highly emitting surfaces is going to be poor whatever the gas species considered.

To quantify how a low-emissivity surface can improve the retrieval sensitivity in the boundary layer, Fig. 4b shows the same Jacobian as in Fig. 4a (sea surface), but for a surface emissivity typical of a desert soil (Salisbury and D'Aria, 1992) for which the spectral emissivity in the range 2195 to 2215 exhibits an increasing behaviour from 0.71 to 0.79. It is immediately seen from Fig. 4b that now the Jacobian shows secondary maxima close to the surface pressure level. This example suggests that we should exploit mostly land surface and low-emissivity satellite soundings to improve the retrieval sensitivity in the boundary layer. However, how well we need to know land surface spectral emissivity to get reliable estimates remains an open issue which is far beyond the objective of this study. In the present work we will focus on sea surface soundings for which Masusda's model (Masuda et al., 1988) provides an accurate and reliable method, for our need for *a priori* knowledge of spectral emissivity.

This said, Fig. 5 shows an example of retrieved N_2O profile for a tropical situation (we simulate a sea surface sounding). The test profile is a climatological profile where the concentration of N_2O has been increased by +5% at all layers. As expected the retrieval just coincides with the first guess in the lower and upper atmosphere, and shows a good agreement with the test profile in the range 700 to 300 hPa.

The quality of the retrieval has been also checked by inspecting the spectral residual. The analysis of the spectral residual (not shown here for the sake of brevity) reveals that the first guess spectrum (i.e. the spectrum computed on the basis of the first guess N_2O profile) is biased to the test one. When we replace the first guess spectrum with the fitted one, the bias is greatly reduced, with the spectral residual points scattered randomly around zero. These tests confirmed that the inversion approach consistently extracted the information contained in the spectral radiance.

The results and discussion above suggest that to check for changes in N_2O concentration we should choose the pressure range 300 to 700 hPa. In fact the better accuracy in terms of rms error (see Figs. 3 and 5) is achieved at 550 hPa, which is also where the N_2O Jacobian peaks.

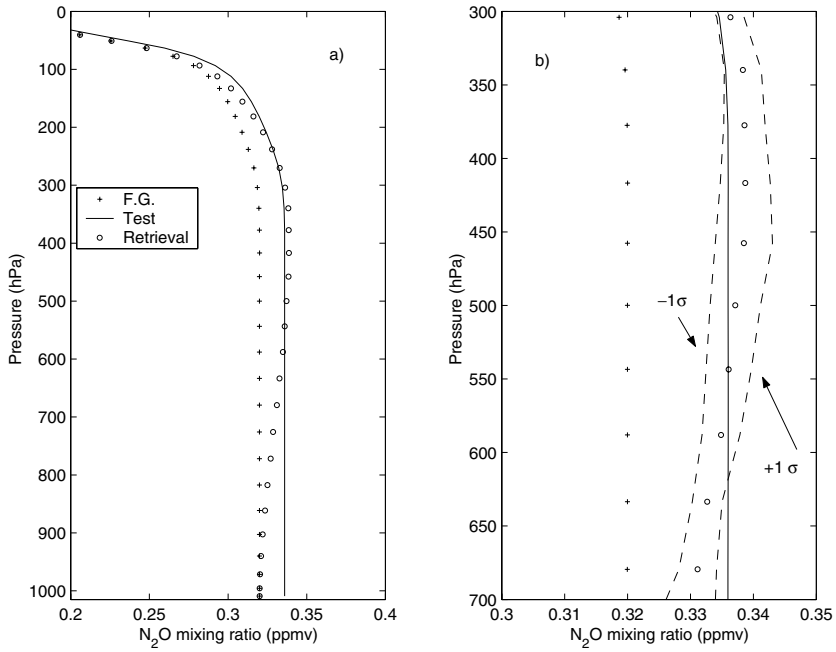

Fig 5. Example of retrieval for a tropical spectrum; (a) first guess (F.G.), test and retrieved profiles are shown for the pressure range 0–1015 hPa; (b) as in (a) but for the pressure range 300–700 hPa; the two dashed curves denote the ± 1 σ tolerance interval.

Table 1. Illustrating the expected retrieval accuracy in the case of a simulated +5% perturbation of the mean climatological N_2O profile. In the case of the non-parametric approach, the retrieval accuracy is that pertaining to the 550 hPa pressure level. For parametric approach, the performance of the method is evaluated in terms of the constant shift parameter, a_s (see text). For both approaches the mean value and rms error of the retrieved mixing ratio (non-parametric approach) and a_s parameter (parametric approach) have been computed on the basis of a sample of 100 retrievals

	Non-parametric retrieval				Parametric retrieval		
Air mass type	First guess (ppmv)	Test value (ppmv)	Expec. value (ppmv)	RMS error (ppmv)	Test value a_s	Expec. value $\langle \hat{a}_s \rangle$	RMS error $\sqrt{\mathrm{var}(\hat{a}_s)}$
Tropical	0.320	0.336	0.337	0.004	0.05	0.049	0.003
Mid-latitude summer	0.320	0.336	0.338	0.003	0.05	0.049	0.003
Mid-latitude winter	0.320	0.336	0.338	0.005	0.05	0.048	0.008
High latitude summer	0.299	0.315	0.316	0.005	0.05	0.050	0.008
High latitude winter	0.320	0.336	0.332	0.009	0.05	0.048	0.016

Table 2. IMG spectra used in the study and the related N_2O mixing ratio estimated on the basis of the non-parametric retrieval approach. F.G., first guess

	IMG observations				N_2O retrieval	
IMG record	Obs.	Lat., Long. (degrees)	Date	UTC	F.G. (ppmv)	Retrieved (ppmv)
374126	2	11.92N, 52.37E	6 May 1997	07:18	0.320	0.3099 ± 0.0036
167229	1	7.39S, 50.63E	12 December 1996	07:14	0.320	0.3346 ± 0.0036
167530	1	12.14S, 26.10W	12 December 1996	12:18	0.320	0.3202 ± 0.0036
327906	1	39.9N, 8.9E	3 April 1997	21:36	0.320	0.3078 ± 0.0053
166921	5	39.61N, 137.95E	12 December 1996	01:57	0.320	0.3242 ± 0.0053

For the numerical exercise described in this section, Table 1 (left-hand side) compares the retrieved values at 550 hPa with the N_2O test concentration as a function of the air mass type. It can be seen that the concentration is retrieved almost unbiased with an accuracy which for the worst case is 3%. Table 2 applies to a perturbation of +5%, the −5% case gives the same results.

3.1.2. Quantifying retrieval interdependency. At the typical spectral sampling of 0.25 cm^{-1} (see Fig. 4a) the N_2O Jacobian does not show any sharp features. It is indeed very smooth and this poses severe limitations on the vertical spatial resolution of N_2O retrieval.

The resolving power or vertical spatial resolution of the spectral radiance is usually addressed in terms of the *a posteriori* covariance matrix, (e.g. Tarantola, 1987). For a given covariance matrix, the larger the off-diagonal elements the worse the spatial resolution, since the parameters have not been independently retrieved from the data set, but only some linear combination of the parameters has been resolved.

To analyse the problem, we form the correlation matrix according to the usual definition:

$$\rho(i, j) = \frac{C(i, j)}{(C(i, i)C(j, j))^{\frac{1}{2}}} \tag{10}$$

where **C** is the *a posteriori* retrieval covariance matrix (eq. 5).

Figure 6 (lower panel) shows the correlation matrix for a typical retrieval example. We see that the dynamic range of the elements of the correlation matrix extends over the whole pressure range. This means that the correlation length scale does not tend to zero. Because of this behaviour, the inversion process can only resolve very smooth vertical structures such as those introduced by a systematic shift in the first guess solution. This perturbation indeed has a length scale tending to infinity and is therefore compatible with the correlation structure of the retrieval.

The high degree of correlation is a consequence of the intrinsically smooth nature of the Jacobian that makes the inverse problem severely ill-conditioned. Also the regularization parameter and the *a priori* constraint which is represented here by the matrix **B**, contribute to a lesser extent to the correlation of the final products. The matrix **B** indeed has a very short correlation length scale, as can be seen in Fig. 6 (upper panel) which shows the mesh surface of the **B** correlation. We see that, in contrast to what happens in Fig. 6 (lower panel), the elements of **B** drop rapidly to zero.

The regularization process might be an additional source of smoothness in the retrieval at the expense of the final spatial vertical resolution. However, we have checked that γ_{opt} ranges mostly in between 0.2 and 2, which is a value at which regularization does contribute to the retrieval but does not dominate the final solution.

Finally, it should be stressed here that the vertical resolution could be improved by increasing the spectral resolution of the radiance.

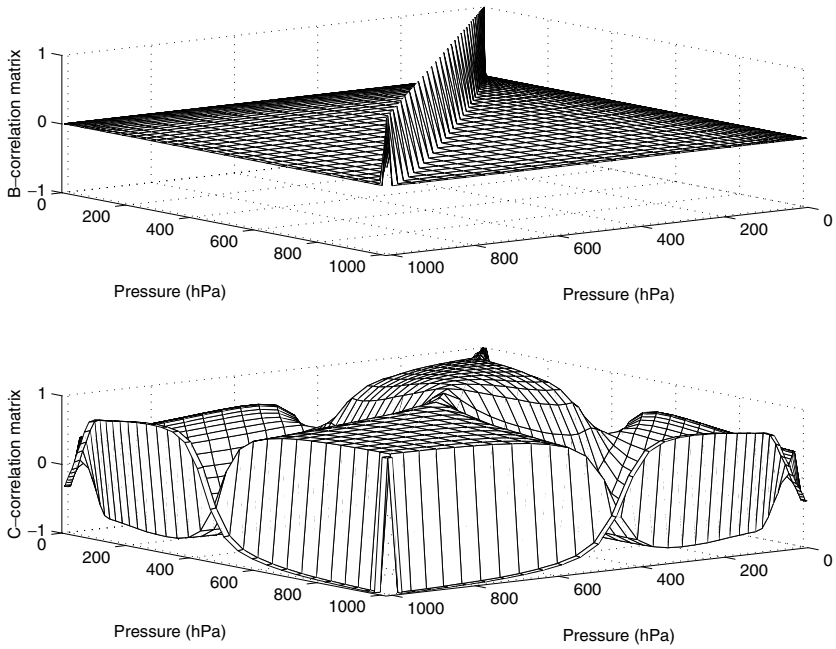

Fig 6. Correlation structure for the **B** matrix (upper panel) and the *a posteriori* covariance matrix (lower panel).

3.2. *Parametric approach to the estimation of N_2O concentrations*

It has been shown in the previous section that the smooth structure of the N_2O Jacobian makes the inversion insensitive to the shape of the profile. In the end, what we can hope to retrieve with a good level of confidence is a constant shift with respect to the reference profile.

Keeping this in mind, we can devise a faster and alternative retrieval algorithm provided that the relation between the observed and reference profile is

$$q(p) = q_0(p)(1 + a_s) \tag{11}$$

where a_s is a constant shift, $q(p)$ is the observed profile and $q_0(p)$ is the reference profile. If we assume the radiative transfer equation to be linear with respect to $q_0(p)$, we can write

$$\begin{aligned} R(i) - R_0(i) &= \sum_{j=1}^{N_1} K(i, j)(q(j) - q_0(j)) \\ &= a_s \sum_{j=1}^{N_1} K(i, j) q_0(j) = a_s x(i) \end{aligned} \tag{12}$$

where $x(i) = \sum_{j=1}^{N_1} K(i, j) q_0(j)$, K is the Jacobian matrix, $R(i)$ is the spectral radiance at wavenumber σ_i, $q(j)$ denotes the concentration at the jth level pressure, N_1 is the number of atmospheric layers, and, finally $R_0(i)$ is the radiance computed at $q_0(j)$.

Using the same vector notation as in Section 3.1, the above equation can be written as:

$$\delta \mathbf{r} = a_s \mathbf{x} \tag{13}$$

and the least squares estimation $\hat{a}_s$ of a_s can be expressed as

$$\hat{a}_s = (\mathbf{x}'\mathbf{S}^{-1}\mathbf{x})^{-1}\mathbf{x}'\mathbf{S}^{-1}\delta\mathbf{r} \tag{14}$$

with the rms error $\delta\hat{a}_s$ given by:

$$\delta\hat{a}_s = \sqrt{(\mathbf{x}'\mathbf{S}^{-1}\mathbf{x})^{-1}}. \tag{15}$$

The above estimation procedure has the advantage of being unbiased, for a perfect linear system, and does not require any kind of regularization.

For the same exercise shown in the previous section (i.e. $\pm 5\%$ perturbation) the approach described here gives the results shown in Table 1 (right-hand side). We can see that this approach gives fairly unbiased results, is able to retrieve the correct amount of shift even for the high-latitude winter atmosphere and is comparable, in terms of N_2O profile accuracy, to the non-parametric approach discussed in Section 3.1.

4. Application to IMG spectra

In this section we consider for illustrative purposes examples of N_2O retrieval examples based on IMG observations. The set of IMG spectra we have used in our analysis is shown in Table 2. We have a total of five spectra, three of which have been recorded in the tropical belt (Indian Ocean and Atlantic Ocean) whereas the remaining two may be classified as mid-latitude winter spectra. Between the last two spectra one has been recorded over the Mediterranean Sea and one over the Sea of Japan. The five observations are intentionally scattered across the globe to serve as a first check of the quality of the current N_2O climatology.

As discussed in Section 2.3, the spectra have been convolved with a Gaussian function and re-sampled at the rate $\Delta\sigma =$

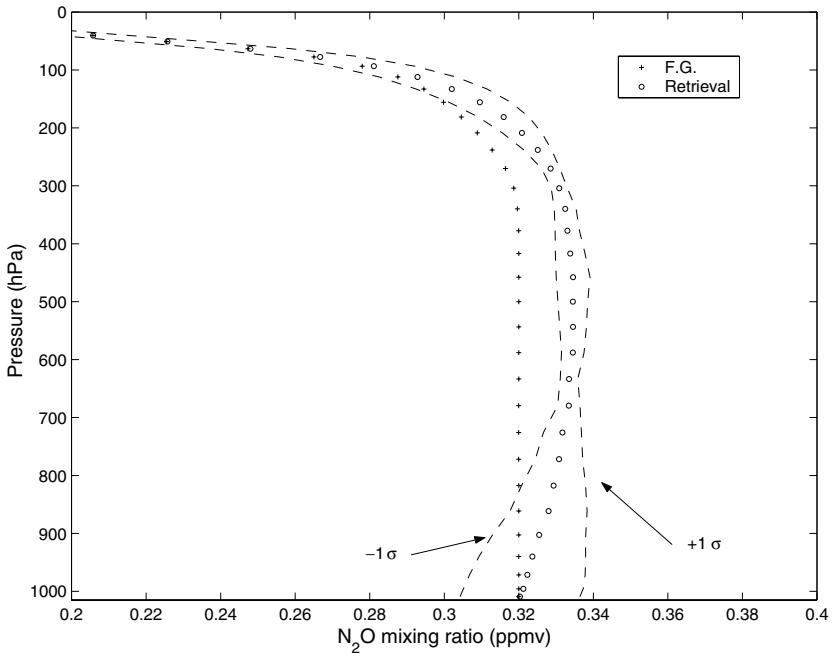

Fig 7. Example of non-parametric retrieval for a tropical IMG spectrum (167229). The $\pm 1\ \sigma$ tolerance interval is shown as a dashed line in the figure. F.G., first guess.

0.25 cm^{-1}. All the spectra are clear sky as shown by co-located Ocean Color and Temperature Scanner (OCTS) imagery.

The analysis at 550 hPa, based on the non-parametric approach described in Section 3.1, gives the results shown in Table 2. It is possible to see that the retrieved quantities fluctuate by 2–5% around the corresponding climatological values, so that no evidence of any serious discrepancy between what is seen in the climatology and what is seen in the retrieval is revealed from the analysis of these data.

An example of non-parametric retrieval for the N_2O profile is shown in Fig. 7 which refers to the tropical IMG spectrum 167229. As expected the retrieved profile coincides with the first guess in the lower and upper part of the atmosphere. Between 300 and 700 hPa, where we expect the highest sensitivity, the

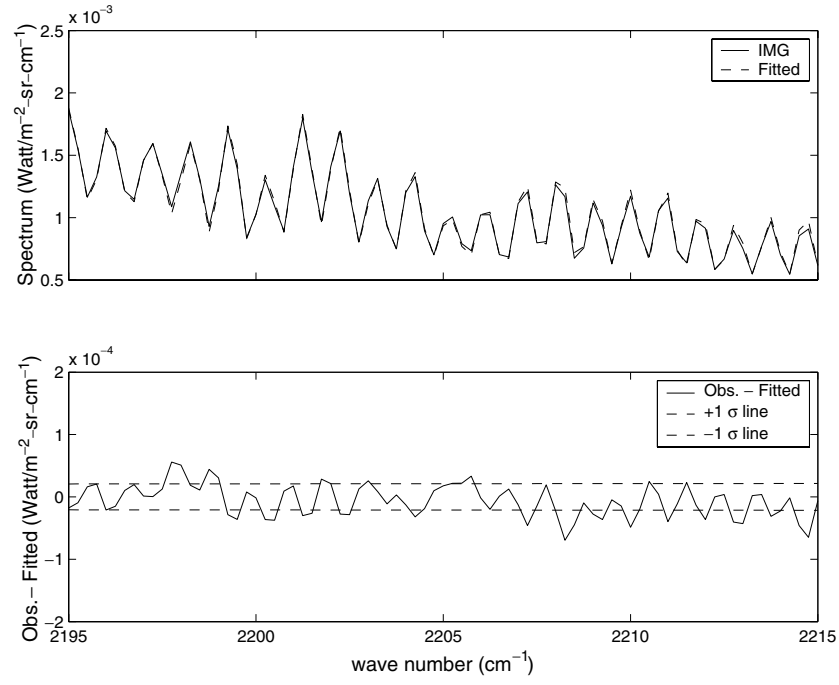

Fig 8. Observed and fitted spectra (upper panel) for the retrieval example shown in Fig. 7. The difference, Obs.–Fitted, is shown in the lower panel where the two solid lines denote the $\pm 1\ \sigma$ tolerance interval (IMG radiometric noise).

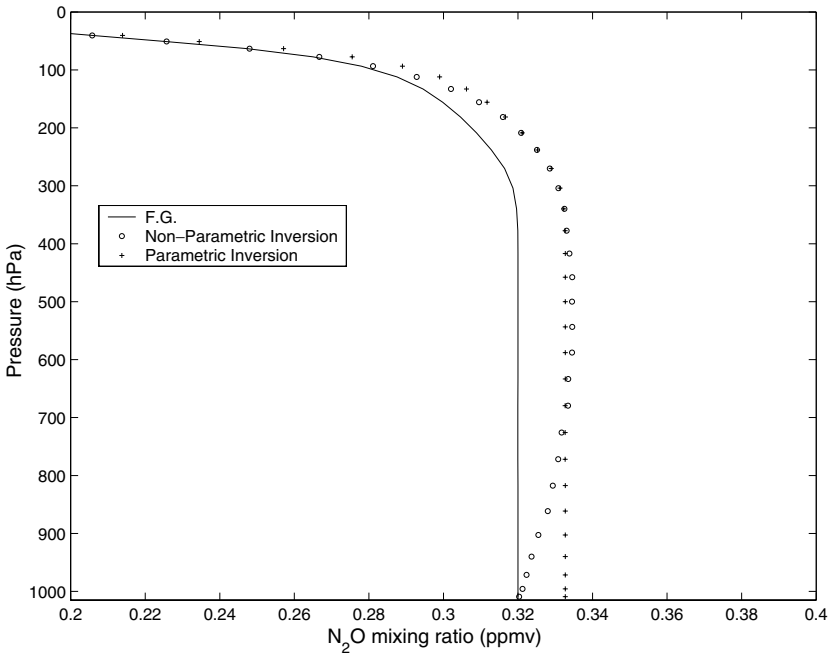

Fig 9. Comparison between the profiles retrieved using the parametric and non-parametric scheme for the tropical IMG spectrum 167229. F.G., first guess.

retrieval indicates an N_2O content that is slightly higher than the climatological value. The discrepancy with climatology is of the order of 4% and is statistically significant as shown by the error bars (see Fig. 7). All the analysed IMG spectra give a retrieved profile that always shows the same pattern: the retrieved profile is the first guess profile scaled by a scaling constant and the retrieval contains no new information about the shape of the observed N_2O profile.

This conclusion is further reinforced when we have a look at the spectral residual, which is shown in Fig. 8. It is seen that the difference between observed and fitted spectra falls mostly in between the $\pm\sigma$ tolerance interval (IMG radiometric noise). This behaviour closely follows what we obtained with numerical exercises, although features are present with real observations which were not seen in the simulations. Even though in principle these could be attributed to errors in the forward model they are more likely to be generated by a discrepancy between the real and assumed IMG instrumental response function. An additional concern with IMG data is their calibration accuracy (e.g. Masiello et al., 2003). Although the data we have used in our analysis have been checked for calibration errors, unresolved phase errors could be present as well. This effect could also explain some of the variability of the data shown in Table 2. However, the IMG data are here used mostly for illustrative purposes and not to draw conclusions about the N_2O variability, which is not the case, also, in view of the limited statistics presented in this study.

Finally, for the case of the IMG spectrum 167229, Fig. 9 compares the parametric with the non-parametric retrieval. The parametric approach estimates a shift of $+0.0396 \pm 0.0033$, which is perfectly in line with the one given by the non-parametric analysis. A look at the two retrieved profiles shown in Fig. 9 shows that exactly the same information is extracted by the two different approaches in the pressure range 300–700 hPa.

5. Conclusions

An inversion strategy to retrieve N_2O from radiance measured by high-resolution infrared sensors has been described. The strategy uses a sequential approach in which, first, temperature and water vapour are retrieved and then N_2O is inverted using the radiance measured in the range 2195–2215 cm^{-1}. Two different schemes have been developed and described. The first one is based on a physical scheme which is optimally regularized using the L-curve criterion (Hansen, 1992). The second one uses a simple parametrization of the observed profile in terms of a reference profile in which only the global amount of N_2O is changed whereas the vertical structure of the profile is left unchanged.

The performance of both methods has been evaluated in simulations using IASI-like spectra for different air mass types. Results show that the N_2O mixing ratio can be retrieved with an accuracy of 1–3%. The sensitivity to N_2O is maximum for pressures between 300 and 700 hPa. Both schemes require the calculation of Jacobians. This is not a serious shortcoming since they can be pre-computed for a set of a reference profiles.

Based on the results discussed in the previous sections we can draw the following conclusions:

- No information for N_2O can be obtained in the boundary layer by using spectra recorded over the sea surface; the retrieval in the boundary layer could be significantly improved by

sensing over a low-emitting land surface, such as desert soil. The reliability of this last approach still remains to be assessed.

- The amount of information that can be obtained regarding the shape of the observed N_2O profile is very limited,
- Reliable information may be obtained for the N_2O total column amount by either a non-parametric or a parametric approach.
- The most appropriate pressure range to check whether or not a constant shift has occurred to the N_2O reference profile is 300 to 700 hPa.

It should be also stressed that the accuracy of 1–3% refers to one single IMG spectrum whose acquisition time is 10 s. In addition, IMG has been operated in nadir mode (no scanning) and the size of its nadir footprint is a square box of 8 km by 8 km. In about 110 s IMG takes a sequence of six soundings which covers a latitudinal line of ≈500 km. Averaging retrieval over these six soundings would improve the accuracy by a factor of $\sqrt{6}$, and still have spatial information useful for climatology. For scanning and multiple-FOV geometry sounders such as IASI and AIRS, the situation is far better. Because of the IASI multiple-FOV geometry, four observations are available at each sounding which may improve the accuracy by a factor of 2 and still have a spatial horizontal resolution of about 24 km. Because of the scanning mode, the accuracy would improve by a factor of 8 if we consider a lower horizontal spatial resolution of 100 km.

Thus, the major concern about N_2O satellite retrieval is not an issue of 1–3% accuracy. New modern sensors, such as AIRS and IASI, will be continuously measuring over the 15-yr lifetime of their mission, which should give records long enough to detect small changes in the average global concentration of N_2O and other greenhouse gases, as well. A major concern is then the instrument stability and possibly unknown biases which are likely to plague indirect measures such as those from satellites. In this respect, the methodology we have described makes no use of ancillary information, e.g. temperature and water vapour, and exploits the given spectral radiance alone. This strategy largely mitigates potential bias whose only source is, therefore, confined to the regularization process. However, this source has been assessed to be minor. Other sources of bias could be introduced by, for example, forward model assumptions such as the *static* pressure grid used for the layering of the atmosphere. This could be a concern for the mixing ratio profile, in which case a possible bias may occur into the attribution of the profile to the right vertical pressure scale. However, while important on meteorological timescale, this would not be a problem on a climatological scale where we may assume that uncertainty in meteorological conditions result in a final random error component which may be filtered out by a proper averaging operation.

Finally, our methodology have been exemplified by considering a few IMG retrieval examples. Results confirm the consistency of the non-parametric and parametric algorithms. Although illustrative, the application to IMG spectra demonstrates that the concept of N_2O retrieval using high spectral resolution infrared observations from satellite-borne sensors does work.

6. Acknowledgment

This work is supported by the Italian Space Agency. Marco Matricardi is supported by EUMESTSAT (contract EUM/CO/01/882/DK) through the IASI pre-launch definition studies.

References

Amato, U., De Canditiis, D. and Serio, C. 1998. Effect of apodization on the retrieval of geophysical parameters from Fourier-transform spectrometers. *Appl. Opt.* **37**, 6537–6543.

Amato, U., Masiello, G., Serio, C. and Viggiano, M. 2002. The σ-IASI code for the calculation of infrared atmospheric radiance and its derivatives. *Environ. Model. Software* **17/7**, 651–667.

Anderson, G. P., Clough, S. A., Kneizys, F. X., Chetwind, J. H. and Shettle, E. P. 1986. *AFGL Atmospheric Concentration Profiles (0–120 km)*. AFGL-TR-86-0110, AFGL (OPI), Hanscom Air Force Base, MA 01736, USA.

Carfora, M. F., Esposito, F. and Serio, C. 1998. Numerical methods for retrieving aerosol size distribution from optical measurements of solar radiation. *J. Aerosol Sci.* **29**, 1225–1236.

Chedin, A., Scott, N. A., Wahiche, C. and Moulnier, P. 1985. The improved initialization inversion method: a high resolution method for temperature retrievals from satellites of the TIROS-N series. *J. Clim. Appl. Meteorol.* **24**, 128–143.

Clough, S. A., Kneizys, F. X. and Davies, R. W. 1989. Line shape and the water vapor continuum. *Atmos. Res.* **23**, 229–241.

Clough, S. A., Iacono, M. J. and Moncet, J.-L. 1992. Line-by-line calculation of atmospheric fluxes and cooling rates, 1, Application to water vapor. *J. Geophys. Res.* **97**, 15761–15785.

Hansen, P. C. 1992. Analysis of discrete ill-posed problems by L-curve. *SIAM Rev.* **39**, 561–580.

Kendall, M. and Stuart, A. 1979. *The Advanced Theory of Statistics*. 2nd edn, Vol. 2, C. Griffin, London.

Kobayashi, H., Shimota, A., Yoshigahara, C., Yoshida, I., Uehara, Y. and Kondo, K. 1999. Satellite-borne high-resolution FTIR for lower atmosphere sounding and its evaluation. *IEEE Trans. Geosci. Remote Sensing* **37**, 1496–1507.

Liou, K. N. 1992. *Radiation and Cloud Processes in the Atmosphere*. Oxford University Press, Oxford, UK.

Lubrano, A. M., Serio, C., Clough, S. A. and Kobayashi, H. 2000. Simultaneous inversion for temperature and water vapor from IMG radiances. *Geophys. Res. Lett.* **27**, 2533–2536.

Masiello, G., Serio, C. and Shimoda, H. 2003, Qualifying IMG Tropical Spectra for Clear Sky. *J. Quant. Spectrosc. Radiat. Transfer* **77/2**, 131–148.

Masuda, K., Takashima, T. and Takayama, Y. 1988. Emissivity of pure and sea waters for the model sea surface in the infrared window regions. *Remote Sens. Environ.* **24**, 313–329.

Rothman, L. S., Rinsland, C. P., Goldman, A., Massie, S. T., Edwards, D. P., Flaud, J.-M., Perrin, A., Camy-Peyret, C., Dana, V., Mandin, J.-Y., Schroeder, J., McCann, A., Gamache, R. R., Wattson, R. B., Yoshino, K., Chance, K. V., Jucks, K. W., Brown, L. R., Nemtchinov, V. and

Varanasi, P. 1998. The HITRAN molecular spectroscopic database and HAWKS (Hitran Atmospheric Workstation): 1996 edition. *J. Quant. Spectrosc. Radiat. Transfer* **60**, 665–710.

Prinn, R. G., Weiss, R. F., Fraser, P. J., Simmonds, P. G., Cunnold, D. M., Alyea, F. N., O'Doherty, S., Salameh, P., Miller, B. R., Huang, J., Wang, R. H. J., Hartley, D. E., Harth, C., Steele, L. P., Surrock, G., Midgley, P. M. and McCulloch, A. 2000. A history of chemically and radiatively important gases in air deduced from ALE/GAGE/AGAGE. *J. Geophys. Res.* **105**(D14), 17751–17792.

Salisbury, J. W. and D'Aria, D. M. 1992. Emissivity of terrestrial materials in the 8–14 μm atmospheric window. *Remote Sens. Environ.* **42**, 83–106.

Tarantola, A. 1987. *Inverse Problem Theory*. Elsevier Science, London.

World Meteorological Organization (WMO) 2001. *WMO Global Atmosphere Watch World Data Centre for Greenhouse Gases*. CD-ROM no. 7. Published by the Japan Meteorological Agency in cooperation with the WMO, available from Japan Meteorological Agency (e-mail: wdcgg@hq.kishou.go.jp).